Coupling of static ultramicromagnetic field with elastic micropillar-structured substrate for cell response

Yue Quan [a], Ziyu Huang [a], Yuxin Wang [a], Yu Liu [a], Sen Ding [a], Qian Zhao [a], Xiuping Chen [b], Haifeng Li [a], Zikang Tang [a], Bingpu Zhou [a,**], Yinning Zhou [a,*]

[a] *Joint Key Laboratory of the Ministry of Education, Institute of Applied Physics and Materials Engineering, University of Macau, Avenida da Universidade, Taipa, Macau*
[b] *State Key Laboratory of Quality Research in Chinese Medicine, Institute of Chinese Medical Sciences, University of Macau, Avenida da Universidade, Taipa, Macau*

ARTICLE INFO

ABSTRACT

Micropillars have emerged as promising tools for a wide range of biological applications, while the influence of magnetic fields on cell behavior regulation has been increasingly recognized. However, the combined effect of micropillars and magnetic fields on cell behaviors remains poorly understood. In this study, we investigated the responses of H9c2 cells to ultramicromagnetic micropillar arrays using NdFeB as the tuned magnetic particles. We conducted a comparative analysis between PDMS micropillars and NdFeB/PDMS micropillars to assess their impact on cell function. Our results revealed that H9c2 cells exhibited significantly enhanced proliferation and notable cytoskeletal rearrangements on the ultramicromagnetic micropillars, surpassing the effects observed with pure PDMS micropillars. Immunostaining further indicated that cells cultured on ultramicromagnetic micropillars displayed heightened contractility compared to those on PDMS micropillars. Remarkably, the ultramicromagnetic micropillars also demonstrated the ability to decrease reactive oxygen species (ROS) levels, thereby preventing F-actin degeneration. Consequently, this study introduces ultramicromagnetic micropillars as a novel tool for the regulation and detection of cell behaviors, thus paving the way for advanced investigations in tissue engineering, single-cell analysis, and the development of flexible sensors for cellular-level studies.

1. Introduction

The extracellular matrix (ECM) and its interactions play a vital role in determining the morphology and behavior of cells, including cell proliferation, metabolism, adhesion, and migration [1]. Numerous factors present in ECM, including its structure, stiffness, and many soluble factors, can directly influence cellular function and phenotype [2,3]. Cells have the remarkable ability to detect the forces exerted by the ECM's structure and convert them into intracellular biochemical signals that regulate the cytoskeleton and gene expression [4]. In recent times, scientists have been exploring various geometries such as mushrooms, nanowires, nanopillars, microtube and micropillars [5–8], as well as different materials and fabrication techniques. Additionally, they have also been studying a wide range of cellular models to gain insights into the interactions between cells and the aforementioned microenvironments (i.e., geometries and materials). The modulation of microscopic and nano-morphology of material surfaces has been shown to be an

extremely powerful tool for regulating cell morphology and function. In a study, the utilization of porous microtubes was found to expedite neurite growth, facilitate the direction of neuronal connections, and establish a robust platform for advancing therapeutic interventions and deepening our comprehension of neural networks [9]. HEK-293 cells cultured on high aspect ratio polythiophene pillars displayed a remarkable alteration in the cell morphology and enhanced membrane capacitance. Notably, there were no detrimental impacts observed on cell proliferation and primary neurons also had well electrophysiology properties and synapse number [5]. The effects of micro- and nano-pattern surfaces on a variety of cell functions have also been studied including epithelial–mesenchymal transition (EMT) of cancer cells [10], tumor-like aggregation and branching of glial cells [11], directional alignment of neurons [12,13], as well as adhesion and migration of fibroblasts [14]. Three-dimensional (3D) culture environments exhibit better cell morphologies than 2D surfaces. The researchers delved into various geometric, specifically, they focused on vertically

---

* Corresponding author.
** Corresponding author.

E-mail addresses: bpzhou@um.edu.mo (B. Zhou), ynzhou@um.edu.mo (Y. Zhou).
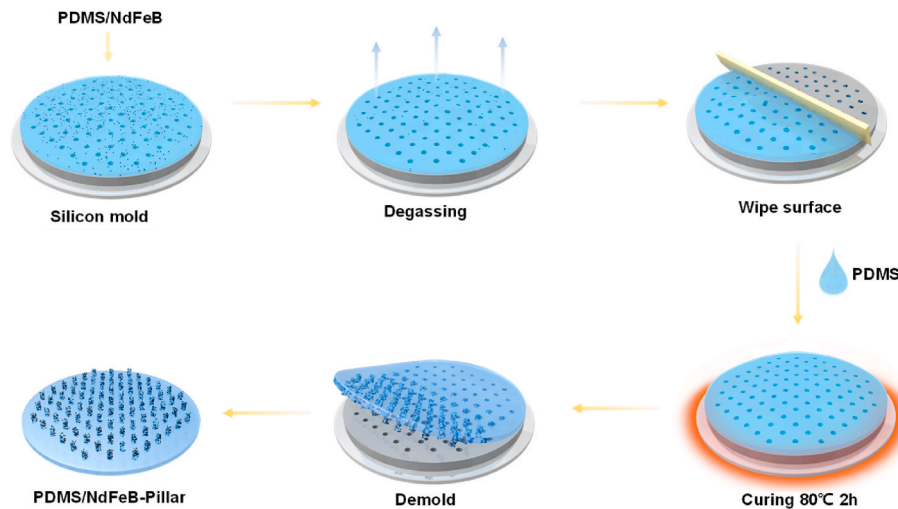
Fig. 1. Ultramicromagnetic micropillar arrays as substrates of H9c2 cells. Schematic representation of magnetic micropillar-fabrication process.

aligned 3D pillar structures that were fabricated using lithography techniques. These structures were evaluated for their suitability in a broad range of biological applications [15]. Some studies revealed that the micropillar structures induced self-deformation of cell nuclei, ultimately influencing their proliferation and adhesion capabilities [16–18].

As an external, non-invasive physical stimulation, the static magnetic field (SMF) has been shown to impact cell function in various ways. For instance, it has been reported to affect the proliferation of 3T3-E1 [19], as well as the proliferation and osteogenic differentiation of mesenchymal stem cells (MSCs) [20–22]. SMF has also been linked to increased proliferative activity of neural progenitor cells (NPCs) [23], and the adhesion and growth of cells [24,25]. The most likely mechanism is mechanotransduction, which converts the persistently weak magnetic forces acting on cells into internal biochemical signals. There are four different categories of magnetic field strength SMF, including weak (<1 mT, i.e. ultramicromagnetic), moderate (1 mT–1 T), strong (1–5 T), and ultrastrong (>5 T) [23]. Given the aforementioned scenario, numerous magnetic materials featuring diverse magnetic field strengths designed for cell usage have been developed in recent years [19,23,25,26]. As these materials possess intrinsic magnetic properties which can augment cell proliferation and adhesion, thereby presenting promising potential applications in the realm of cell biology. Across numerous academic domains, a common assumption has been that the energies linked to weak magnetic fields (WMF) are too trivial to hold biological significance. Nevertheless, several studies have reported that WMF can, in fact, impact biological systems in diverse ways. WMF (100 µT) can reduce the apoptosis, proliferation and necrosis of rat kidney cells, but increase these in astrocytes cells [27]. It was also found that WMFs (200 µT) can alter stem cell proliferation and differentiation through ROS accumulation and heat shock protein 70 expression [28]. Additionally, a separate study has indicated a slight increase in oxidative stress associated with weak SMF (WSMF) (0–600 µT) exposure, while concentrations of superoxide and NO decrease [29]. However, there has been limited research conducted on the effects of WSMF on cell cultures, leaving the precise mechanisms by which WSMF (<1 mT, i.e., ultramicromagnetic) interacts with cells largely unknown. For the first time, we combined the ultramicromagnetic field with the micropillar structure to explore the role of the ultramicromagnetic field in the interaction between cells and substrate morphology.

Therefore, in this study, the primary objective is to investigate the influence of magnetic 3D structures on cell function with WSMF. We have embedded sufficient NdFeB particles into PDMS to fabricate a novel magnetic micropillar array. These micropillars were then magnetized using a magnetizer to transform each one into a tiny permanent magnet with WSMF of approximately 80 µT. Cardiovascular disease ranks among the foremost global health concerns. Cardiomyocytes, as the pivotal muscle cells responsible for heart ventricular contraction and relaxation, hold paramount importance. Consequently, comprehending the mechanical and physical attributes of cardiomyocytes assumes critical significance. Adhesion of cells to the sensor surface can affect the contractility of cardiomyocytes [30]. Moreover, the three-dimensional microenvironment plays a pivotal role in governing the maturation response of cardiomyocytes induced by their surroundings [6,31]. Thus, in our investigation, we employed H9c2 cardiomyoblasts as the subject of study to explore the effects of the magnetic micropillars on the cells. We first explored the impact of WSMF combined with topography on the biological behavior of H9c2 cells. The results showed that the micropillar substrates induced the morphological change and nuclear deformation in H9c2 cells. Ultramicromagnetic micropillars have been found to enhance cell proliferation, adhesion, and cytoskeleton remodeling, compared to the pure PDMS micropillars.

2. Materials and methods

2.1. Fabrication of magnetic micropillar arrays

A silicone female template for casting micropillar array substrates was fabricated by Deep Silicon Etching. PDMS, curing agent and NdFeB were mixed at a 10:1:10 ratio. The mixture was degassed under vacuum for ~5 min and was cast onto the silicon mold. Then, the excess of mixture on the surface has been wiped to observe the cells growing on the micropillars by optical microscope. Then, a normal PDMS solution was poured over the template and degassed under a vacuum for ~5 min. The whole device was cured at 80 °C for 2 h. A micropillar array substrate was then peeled away from the template. The micropillar array substrate was finally magnetized by a commercial magnetizer (MA-3030, Jiu Juok, Shenzhen, China) under a constant magnetic field of ~3 T to obtain the magnetic micropillars. In this study, the pillar diameter D was 5 µm, and their length L was 10 µm. The center-to-center spacing of the pillars was 15 µm (Fig. 1).

2.2. Cell culture

H9c2 rat cardiomyoblasts were purchased from MINGZHOUBIO (B164546, Ningbo, China) and cultured on micropillar arrays with Dulbecco's Modified Eagle's Medium (DMEM, Gibco, USA) containing 10 % fetal bovine serum (FBS, Gibco, USA) Glutamine (2 mM), penicillin (100 units/mL), and streptomycin (0.1 mg/mL) at 37 °C in a humidified 5 % CO_2 incubator. Before culturing cells, micropillar plates were UV-
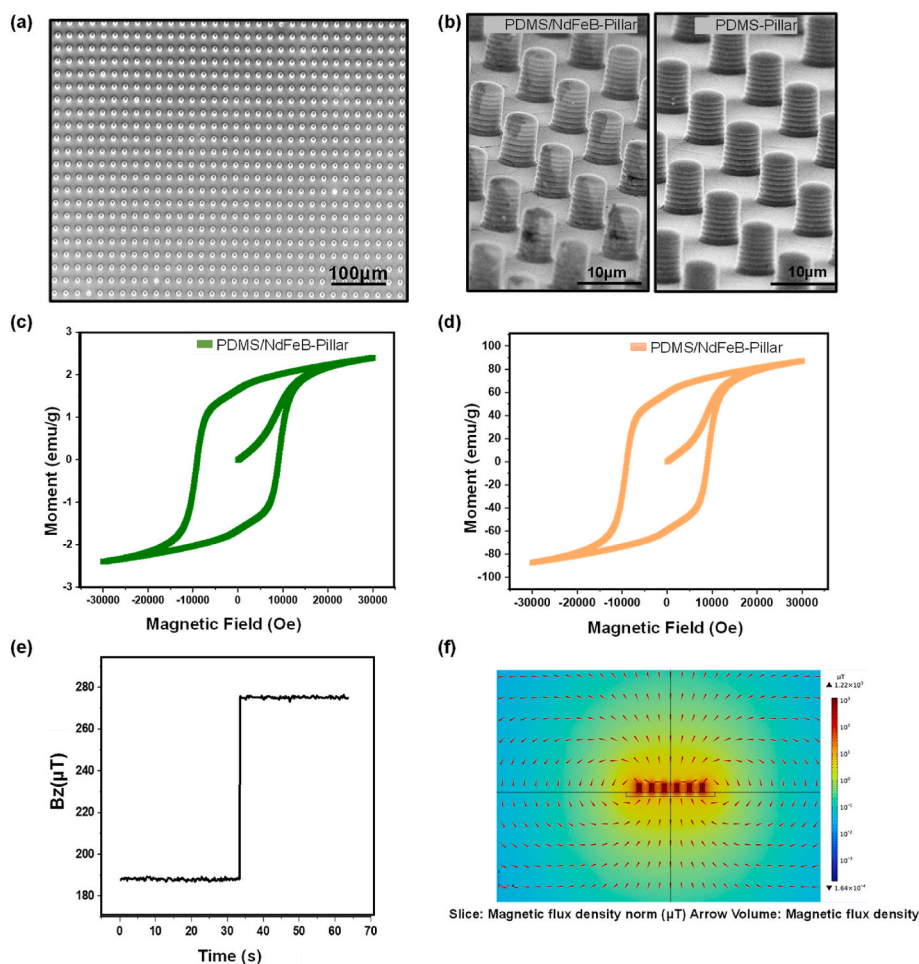
Fig. 2. Characteristics of ultramicromagnetic micropillar. (a) SEM images of the magnetic micropillar arrays (Scale bar, 100 μm) and the (b) PDMS/NdFeB micropillars and PDMS micropillars (Scale bar, 10 μm). (c) Hysteresis loop of PDMS/NdFeB micropillars with PDMS substrate and (d) PDMS/NdFeB bulk composite. (e) The magnetic field of magnetic micropillar arrays measured by Hall sensor. The first 30s is no-load, and the second 30s is to put the magnetic micropillar arrays on the sensor (f) Simulation results of the ultramicromagnetic field distribution around the magnetic micropillar arrays.

sterilized for 1 h and incubated with the 10 μg/mL Fibronectin (F8180, Solarbio, Beijing, China) for 1 h. The H9c2 cells were then plated on flat, PDMS-Pillar and NdFeB/PDMS-Pillar groups at a density of 5×10^5 cells/well, respectively.

2.3. Reactive oxygen species (ROS) levels in vitro

H9c2 cells were cultured on the different micropillar groups and flat substrate for 48 h, respectively. Then, cellular ROS levels were detected using a DCFDA-Cellular ROS Detection Assay Kit (CA1410, Solarbio, Beijing, China). According to the instructions of the manufacturer, 10 μM 2′,7′-dichlorofluorescin diacetate (DCFDA) was added at 37 °C for 30 min, and fluorescence was measured using an inverted fluorescence microscope (Olympus, Japan) and Flow cytometer (Miltenyi, MACS-Quant, Germany).

2.4. Cell viability and proliferation analysis

Cell viability was checked after 48h culture on the micropillars using LIVE/DEAD Cell Imaging Kit (R37601, Invitrogen, USA) by inverted fluorescence microscope. CCK-8 Assay Kit (CA1210, Solarbio, Beijing, China) was used to examine the cell proliferation assay.

2.5. Staining of cells and morphological observations

A warm phosphate-buffered saline (PBS) solution was used to wash cells. Then the cells on the micropillar with or without micropillar arrays were fixed in 4 % paraformaldehyde for 15 min and permeabilized with 0.3 % v/v Triton X-100 with 1 % bovine serum albumin (BSA) for another 30 min. In order to label the filamentous actin (F-actin), we incubated the cells with 1 μg/mL Phalloidin-FITC (CA1620, Solarbio, Beijing, China) at room temperature for 30 min. We labeled cell nuclei with 4′,6-diamidino-2-phenylindole (DAPI) (S2110, Solarbio, Beijing, China) for 5 min. All samples were imaged using a Zeiss LSM 710 confocal microscope.

2.6. Immunofluorescence staining

After 48 h culture in the growth medium, PBS solution was used to wash cells. Then, cells on the micropillar with or without micropillar arrays were fixed in 4 % paraformaldehyde for 15 min and per-meabilized with 0.3 % v/v Triton X-100 with 1 % bovine serum albumin (BSA) for another 30 min. For immunostaining of α-actinin and Con-nexin 43, the cells were incubated with 1:1000 diluted primary antibody of mouse monoclonal anti-α-actinin (#69758, Cell Signaling Technol-ogy, USA) and Rabbit monoclonal anti- Connexin 43 (#3512, Cell Signaling Technology, USA) at 4 °C overnight. After thoroughly rinsed with PBS, the cells were further treated with secondary antibody Alexa
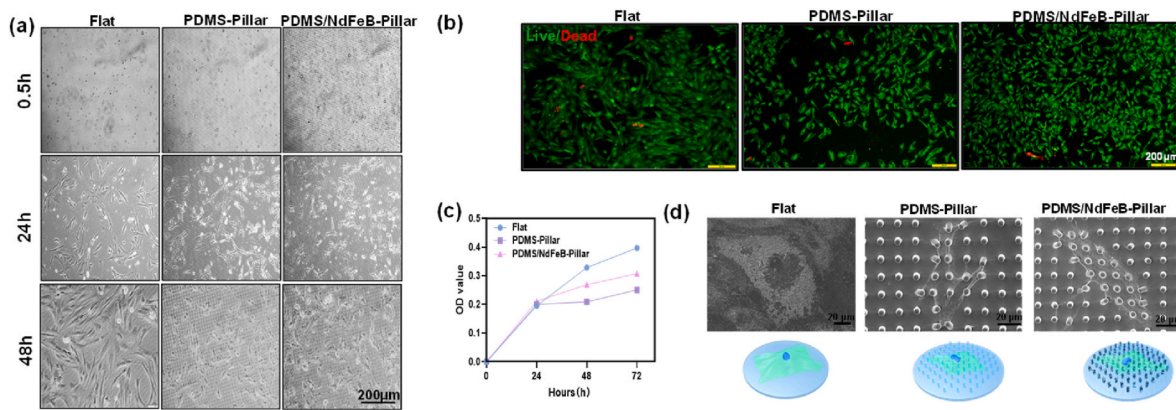
Fig. 3. The morphology and growth of H9c2 Cells on the micropillar arrays and flat substrates. (a) The image of cell morphology and number changes along with the time on different substrates under bright field (Scale bar, 200 μm). (b) After 48h culture on different substrates, the viability of H9c2 determined by LIVE/DEAD kit, live (green), dead (red) (Scale bar, 200 μm). (c) H9c2 cell proliferation curve detected by CCK-8 kit. Each group started with the same number of cells. (d) SEM images and schematic diagram of H9c2 cells growing on the micropillars and flat substrates (Scale bar, 20 μm).

Fluor 488-conjugated goat anti-mouse IgG and Alexa Fluor 555-conjugated goat anti-rabbit IgG (#4480, #4413, Cell Signaling Technology, USA) diluted by 1:1000, and incubated at room temperature for 1 h. Moreover, nuclei were labeled as described in the above section. All samples were imaged using a Zeiss LSM 710 confocal microscope.

2.7. ProteinSimple capillary electrophoresis immunoassay

ProteinSimple capillary-based immunoassay (Jess system, ProteinSimple, San Jose, CA) is an automated capillary size separation and nanoimmunoassay system that incorporates and automates the entire protein separation and detection process using homemade antigens. According to the manufacturer's protocol, the samples were mixed with the fluorescent 5 × master mix (ProteinSimple) and then heated at 95 °C for 5 min. Boiled samples, biotinylated protein ladder, blocking buffer, primary antibodies, ProteinSimple horseradish peroxidase-conjugated anti-rabbit or anti-mouse secondary antibodies, luminol-peroxide and wash buffer were loaded into the designated wells plate (12–230 kDa Pre-filled Plates with Split Buffer, ProteinSimple). The α-actinin primary antibodies were diluted at 1:50. The plates and capillary cartridges were loaded into the instrument. Digital images were analyzed using Compass for SW software.

2.8. The formula of four shape descriptors in cell nuclei

Circularity or **Roundness** is a measure of how closely the shape of an object approaches that of a perfect circle. It is calculated as the ratio of the area of an object to the area of a circle with the same perimeter. This value equals 1 for a circular object and less than 1 for others. **Aspect ratio** is a measure of how elongated or flattened an object is. It is calculated as the ratio of the maximum length to the minimum length of an object. This value equals 1 for a square or circular object and greater than 1 for an elliptical or rectangular object. **Solidity** is a measure of how convex or concave an object is. It is calculated as the ratio of the area of an object to the area of its convex hull. This value equals 1 for a convex polygon or circle and less than 1 for others.

2.9. Statistical analysis

All experiments were performed with at least three replicates per group. The data shown are representative of these experiments and are presented as the mean ± SD. Statistical differences were analyzed using a *t*-test. Statistical analysis was conducted using GraphPad Prism 7.0 software, and statistical significance was declared as $*p < 0.05$, $**p < 0.01$ and $***p < 0.001$ vs Flat group, $\#p < 0.05$, $\#\#p < 0.01$ vs PDMS-Pillar group.

3. Results

3.1. Fabrication and characterization of PDMS/NdFeB-pillar

The PDMS/NdFeB-Pillar were fabricated on PDMS films for high transparency to facilitate observing the cells growing on the micropillars by optical microscope. The finer details of the micropillars were clearly displayed through SEM. Some representative images of the micropillar array are shown in Fig. 2a and b. The images demonstrated that micropillars have a diameter of 5 μm, spacing of 15 μm, and height of 10 μm. The dimensions of the micropillars were confirmed to be appropriate for cells to grow on the pillar surface, as shown in Fig. 3a, d for the inverted microscope bright field and SEM images of H9c2 cells on the micropillar array.

Due to the large coercive field and remanence strength of NdFeB and the biocompatibility of PDMS, NdFeB particles and PDMS were mixed to realize the flexible magnets that can be used in biomedicine [32,33]. The M − H curve of the PDMS/NdFeB-Pillar (Fig. 2c) and PDMS/NdFeB composites (Fig. 2d) were measured by a physical property measurement system (PPMS) (see Fig. S1 of the samples for the hysteresis measurement). Regarding with the magnetic particle concentrations, we have explored the cell proliferation after 48h cell culture on different substrates. We found that different ratio (1:1 or 1:2) of PDMS: NdFeB micropillar had no significant difference in cell proliferation (Fig. S2). However, the higher NdFeB ratio (1:2) would increase the micropillar elastic modulus (Fig. S2 of the elastic modulus formula), which was not conducive to mold perfusion. Thus lead to the great difficulty on template demolding and cannot maintain pillar structures, therefore a 1:1 ratio of NdFeB to PDMS was selected in this study. In order to determine the specific magnetic field range of the micropillars, the Hall element is used to detect the magnetic field of the PDMS/NdFeB-Pillar. As shown in Fig. 2e, (see Fig. S3 of the Hall element detection method), the magnetic field is approximately 80 μT. Fig. 2f also shows the simulation results of the magnetic field distribution around the PDMS/NdFeB-Pillar (see Method S1 of simulation method).
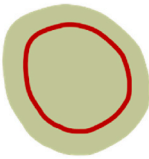
#### 3.2. The morphology and growth of H9c2 cells on an ultramicromagnetic micropillar array

Morphology is an important index for cell growth. H9c2 cells adhere to flat culture plates forming a monolayer of tightly compact cells that indicates healthy (Fig. 3d). Flat and micropillar arrayed substrates could maintain both the normal growth and adhesion of cells. Fig. 3a compares
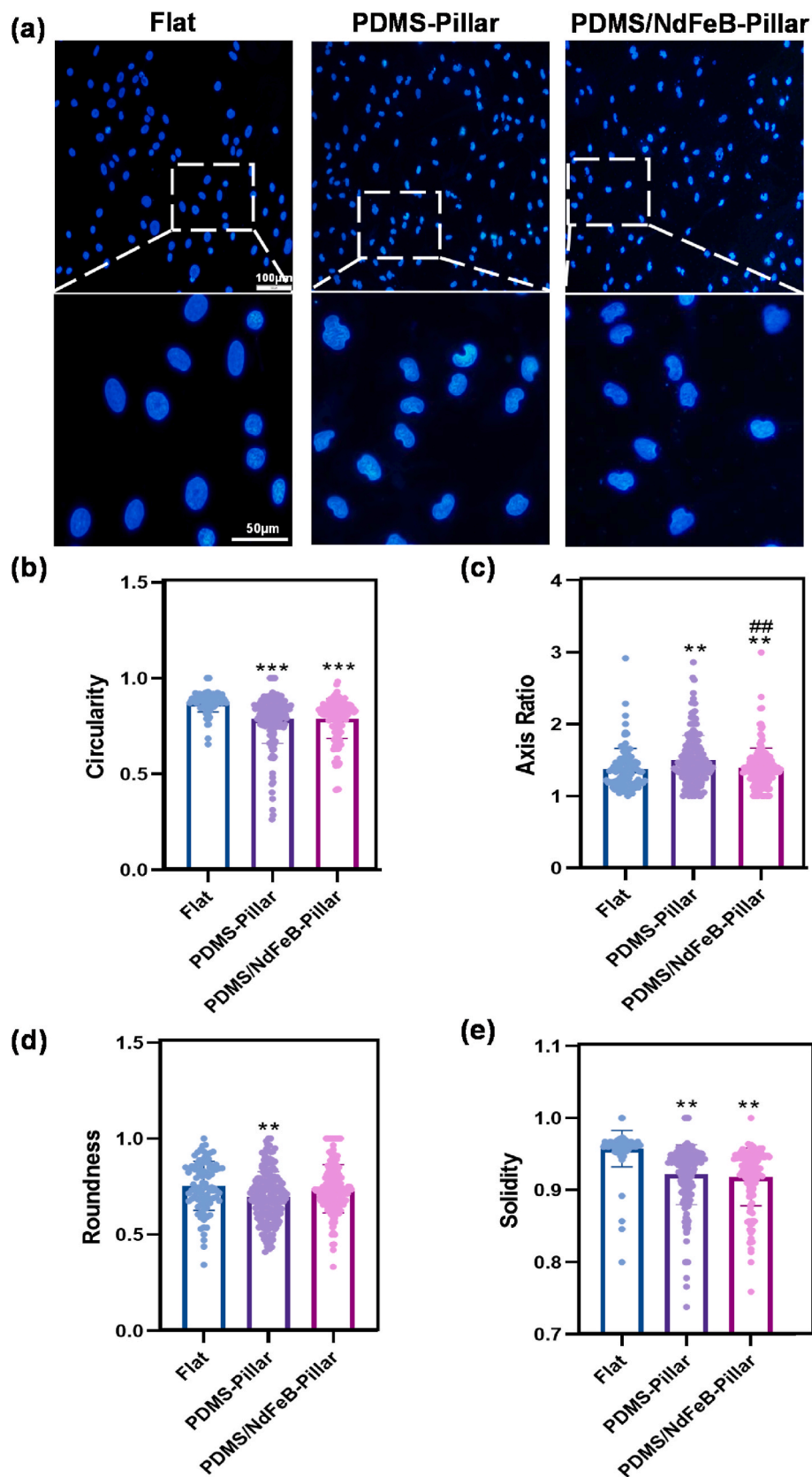
Fig. 4. Nuclear responses of H9c2 cells grown on the micropillar arrays and flat substrates. (a) Representative confocal fluorescence micrographs of nuclei in blue of H9c2 cells with various grown substrates at 48h culture time respectively. Comparisons of parameters (b) circularity, (c) axis ratio, (d) roundness, and (e) solidity; (N = 100); **P < 0.01, ***P < 0.001 vs Flat. ##p < 0.01 vs PDMS-Pillar.

Table 1
The formula of four shape descriptors and hypothetical distortions in undeformed.

Nucleus	Circularity	Aspect ratio	Roundness	Solidity
	$\dfrac{4\pi \times [\text{Area}]}{[\text{Perimeter}]^2}$	$\dfrac{[\text{Major Axis}]}{[\text{Minor Axis}]}$	$\dfrac{4 \times [\text{Area}]}{\pi \times [\text{Major axis}]^2}$	$\dfrac{[\text{Area}]}{[\text{Convex Area}]}$
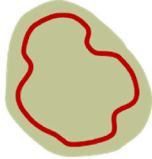
time-dependent morphological changes in H9c2 cells grown on a flat substrate and two types of micropillar arrays (i.e., PDMS/NdFeB-Pillar and pure PDMS-Pillar). While H9c2 cells grown on a flat substrate formed clusters of cells with a spindle-to-stellate-shaped morphology when cultured for a long time, those grown on micropillar arrays became markedly elongated and smaller. The morphology of cells grown on micropillar arrays exhibited distortion, the cell adhesive area was reduced, and the micropillars were stirred by the close connection between the cells and the micropillars. The morphology of cell growth on the flat and micropillar substrates observed by SEM was shown in Fig. 3d.

There was no significant cell death (red) in each group indicating that the PDMS/NdFeB-Pillar array possesses great biocompatibility (Fig. 3b). To further evaluate the effects of different substrate morphology on cell proliferation and viability, we compared the proliferation of cells grown in each group. H9c2 cells were cultured in flat and micropillar plates for 72 h, and it was found that there was a significant difference in cell proliferation between the flat group and micropillar arrays (Fig. 3c). It is noteworthy that magnetic PDMS/NdFeB-Pillars can positively modify cell proliferation compared to PDMS-Pillars.

Consistent with the above, static magnetic fields can ameliorate cell proliferation even in the presence of ultramicromagnetic fields (<0.1 mT).
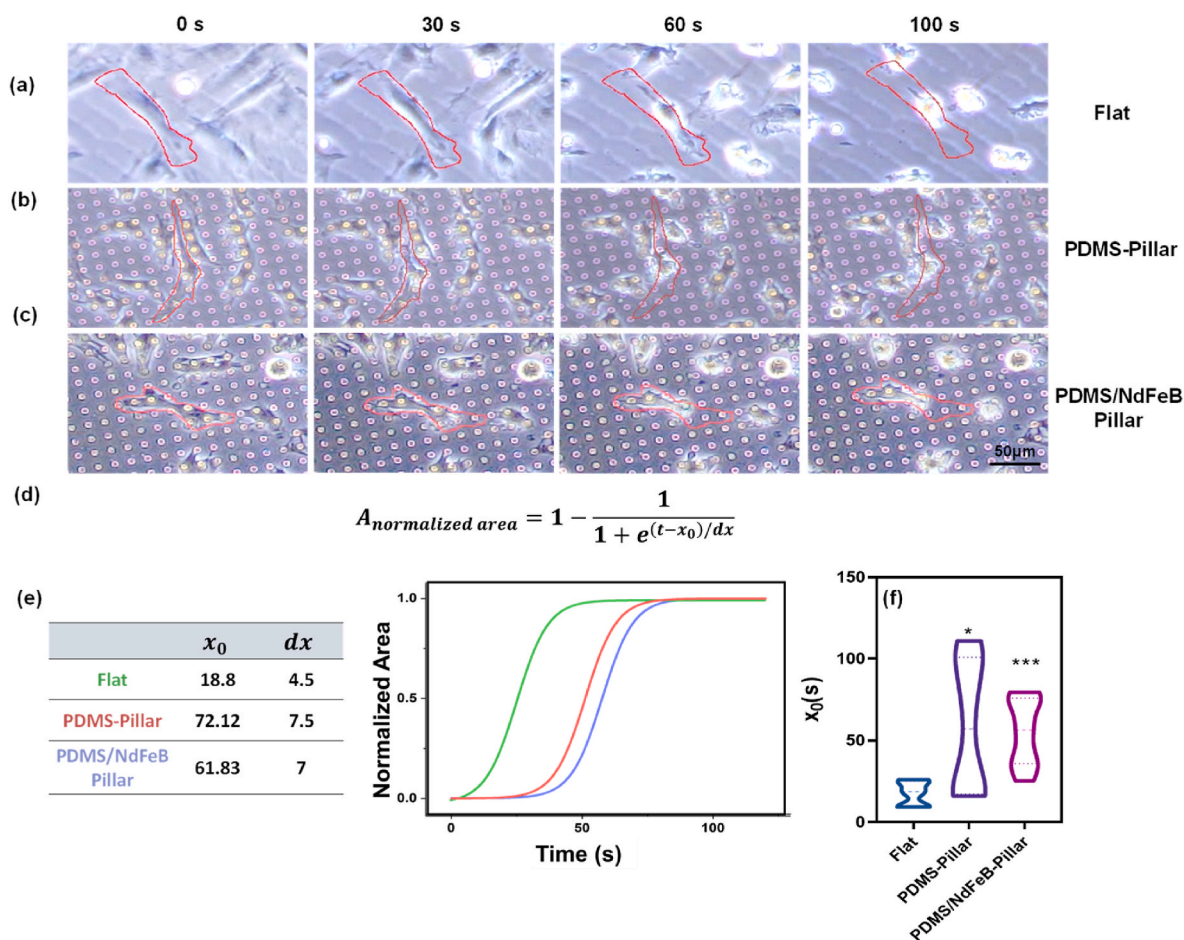
3.3. Micropillar array leading to self-deformation of cell nuclei

The micropillar arrays were reported to deform nuclei, the largest and stiffest organelle in a cell, which plays a vital role in regulating cell behavior [34,35]. The H9c2 cells cultured on flat and micropillars substrates were fluorescently stained to investigate the nuclear responses. As shown in Fig. 4a, the representative confocal fluorescence images presented the nuclei (blue) of the cells which were cultured for 48h in a growth medium. Cells grown on the micropillar exhibited obvious nuclear deformation compared to the flat substrates. The quantitative analysis of the nucleus shape distortions was calculated by the following shape descriptors: circularity, roundness, solidity, and aspect ratio and these four descriptors are dimensionless (Table 1). The

related results were presented in Fig. 4 b-e. Circularity is a measure of how close a cell nucleus to a perfect circle; circularity of 1.0 indicates a perfect circle whereas the value approaches 0.0 means an increasingly elongated shape. The circularity values were around 0.90 in cells cultured on the flat substrates. On the micropillar array, however, circularity values were substantially lower and close to 0.70 indicating the cell nuclei deformed severely. Compared with the flat group, the micropillar groups with or without a WSMF had lower roundness, solidity and higher aspect ratio. These data confirmed that the micropillar induced the deformation of the cell nuclei, and the WSMF did not provide obvious effects on the cell nuclei deformation induced by the topography in macroscopic scales.

### 3.4. Biophysical characteristics of H9c2 cells grown on micropillar arrays

Cell adhesion and contractility are important biophysical states of the cell. To explore the biophysical properties of the cells grown on ultramicromagnetic micropillars, we first performed a trypsin-induced deadhesion assay-an excellent tool for exploring cell biophysical properties, as shown in Fig. 5. For the deadhesion experiment, the cells were incubated with trypsin–EDTA. The cells were imaged at intervals of 10 s until the cells became round and detached (see Fig. S4 of the detailed instructions). As shown in Fig. 5a–c, the cells grown on the flat substrates took less time to shrink and detach than those on micropillars. The temporal change of the normalized cell area was fitted with the Boltzmann sigmoidal equation, which yielded time constants x_0 (cell–substrate adhesion) and dx (contractility) (Fig. 5d). The calculated parameters were shown in Fig. 5e. The longer x_0 meant the stronger cell adhesion, and the shorter dx, illustrated the higher contractility. Thus, these data suggested that the cells cultured on the micropillar array obtained stronger adhesion and less contractility compared to those cultured on the flat plate. Although all the data indicating that weak magnetic fields do not appear to significantly affect cell biophysical properties on a macroscopic scale (which may not be sensitive enough to reflect the influence of ultramicromagnetic fields), such as cell adhesion and nuclei deformation. We further explored the effects of the ultramicromagnetic micropillar arrays on the detailed biochemical properties of H9c2 cells.

$$A_{normalized\ area} = 1 - \frac{1}{1 + e^{(t-x_0)/dx}}$$

	x_0	dx
Flat	18.8	4.5
PDMS-Pillar	72.12	7.5
PDMS/NdFeB Pillar	61.83	7

Fig. 5. Deadhesion dynamics of H9c2 cells on flat, PDMS-Pillar and PDMS/NdFeB-Pillar substrates. (a, b, c) Images of deadhesion of the H9c2 cells on (a) flat, (b) PDMS-Pillar and (c) PDMS/NdFeB-Pillar surfaces (Scale bar, 50 μm). Red dotted lines indicate the area of the cells at different time. Scale bar: 50 μm. (d) Data analysis using Boltzmann sigmoid equation. (e) Normalized area of the representative cells on flat and micropillar surfaces as a function of time. Data were fit to a Boltzmann sigmoidal curve. The x_0 and dx values of representative curve are in the table of (e). (f) Violin plots of x_0 on flat and micropillar array (N = 8). *P < 0.05, ***P < 0.001 vs Flat.
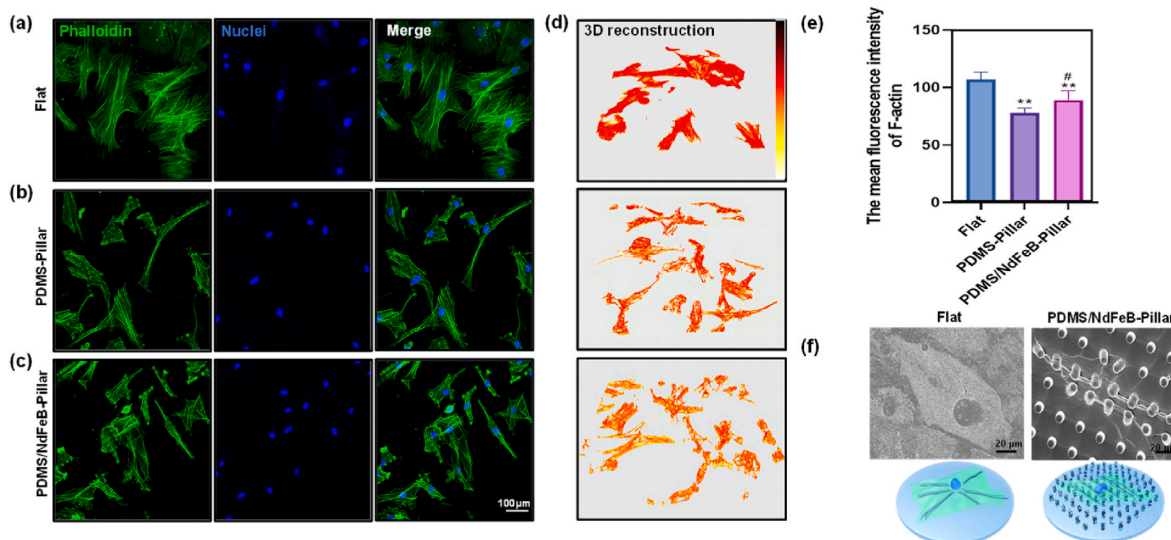
Fig. 6. The cytoskeleton of H9c2 Cells on flat, PDMS-Pillar and PDMS/NdFeB-Pillar. (a, b, c) Representative confocal microscopic images of H9c2 cells after 48 h culture on (a) flat, (b) PDMS-Pillar and (c) PDMS/NdFeB-Pillar (Scale bar, 100 μm). F-actin (green) and cell nuclei (blue) were visualized through fluorescent staining. (d) Fluorescence micrographs captured by scanning along the Z direction were used to construct cell 3d reconstruction. (e) The mean fluorescence intensity of F-action in H9c2 cells seeded for 48 h, on flat, PDMS-Pillar and PDMS/NdFeB-Pillar. **P < 0.01 vs Flat. #p < 0.05 vs PDMS-Pillar. (f) SEM image and schematic illustration of elongated and arranged actin stress fibers on flat and micropillar arrays (Scale bar, 20 μm).
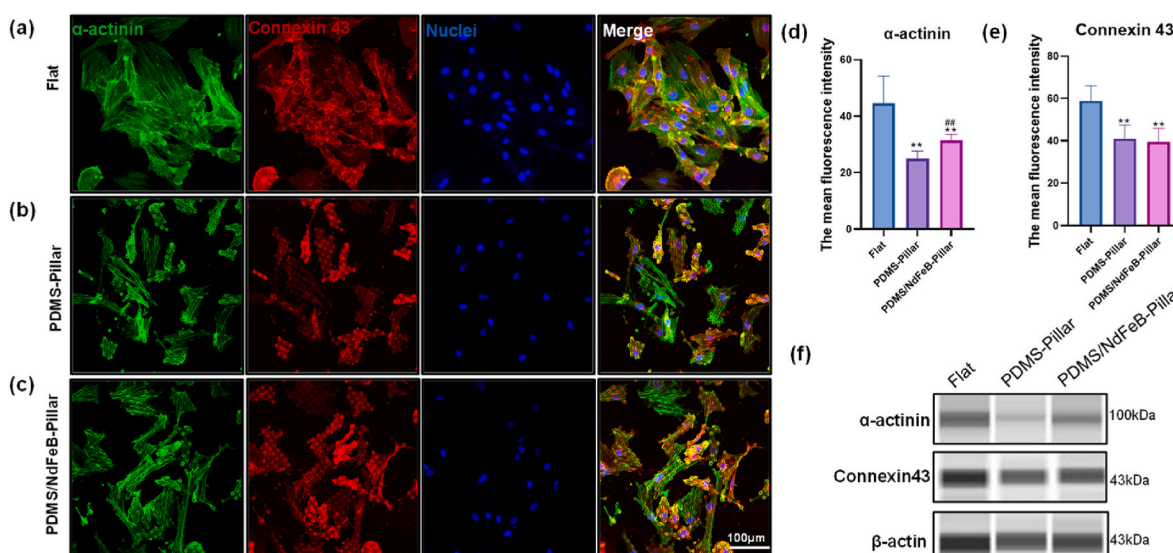
Fig. 7. The Expression of α-actinin, and Connexin 43 in Cells on flat, PDMS-Pillar and PDMS/NdFeB-Pillar. (a, b, c) Representative confocal microscopic images of H9c2 cells after 48 h culture on (a) flat, (b) PDMS-Pillar and (c) PDMS/NdFeB-Pillar (Scale bar, 100 μm). α-actinin (green), Connexin 43 (red) and cell nuclei (blue) were visualized through immunofluorescent staining. (d, e) The mean fluorescence intensity of α-actinin (d) and Connexin 43 (e) in H9c2 cells seeded for 48 h, on flat, PDMS-Pillar and PDMS/NdFeB-Pillar. **$P < 0.01$ vs Flat. ##$p < 0.01$ vs PDMS-Pillar. (f) α-actinin and Connexin43 protein levels determined by capillary electrophoresis immunoassay.

3.5. The cytoskeleton changes of H9c2 cells on ultramicromagnetic micropillar arrays

The deadhesion dynamics highly depends on the structure and mechanics of the intracellular cytoskeleton. Actin is a family of abundant and highly conserved cytoskeletal proteins in all eukaryotic cells [36]. Thus, the cytoskeleton of respective groups were observed after seeding for 48h by stained the F-actin with phalloidin-FITC in Fig. 6a-c. It was found that the area of the cells on the micropillar substrates decreased substantially compared to the flat substrate. The results showed that the area of cells on the micropillar substrate decreased significantly compared with that on the flat, and the shape of cells changed significantly, becoming slenderer and presented thickness enhancement in Z direction, the micropillars appear imprinted into the cytoskeleton.
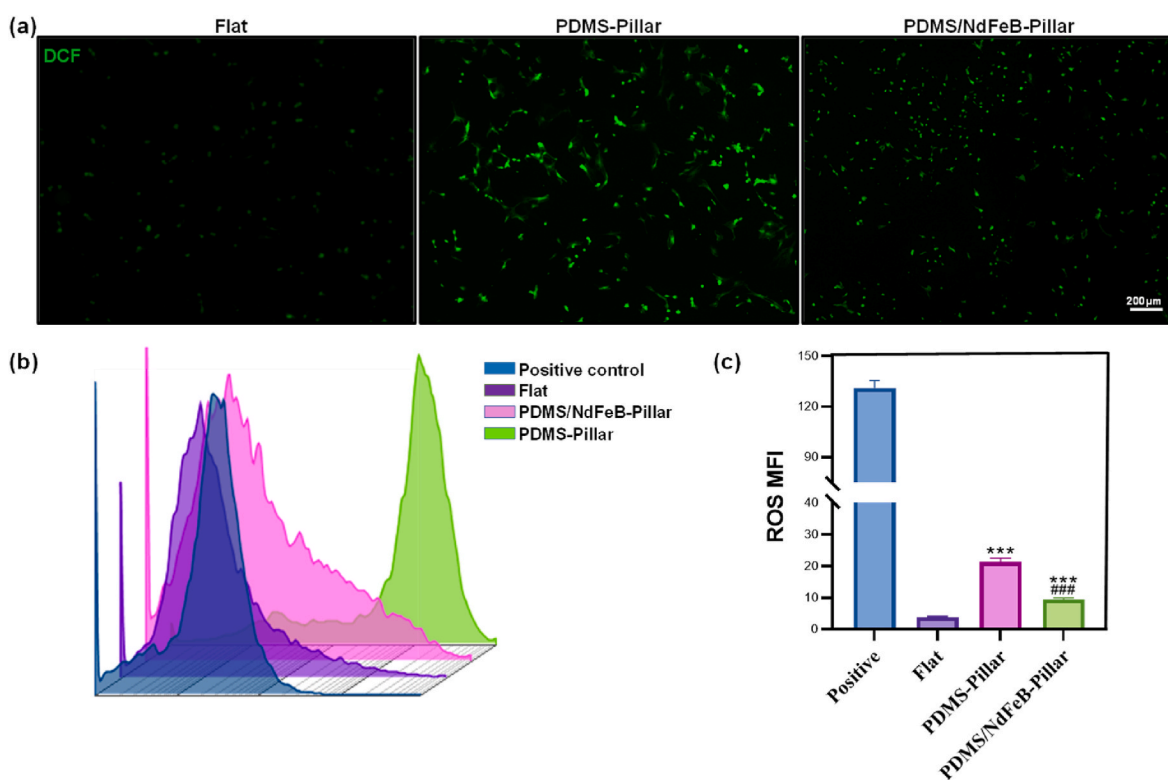
Fig. 8. The ROS level in Cells on flat, PDMS-Pillar and PDMS/NdFeB-Pillar. (a, b) Representative confocal microscopic image of H9c2 cells loaded with DCFH-DA for 30 min (Scale bar, 200 μm), DCF fluorescence intensity was measured by (b) flow cytometry. (c) The mean fluorescence intensity of ROS in H9c2 cells seeded for 48 h, on flat, PDMS-Pillar and PDMS/NdFeB-Pillar. ***$P < 0.001$ vs Flat. ###$p < 0.001$ vs PDMS-Pillar.

Unlike cells that grown on the flat adhering to each other, the boundaries between cells on micropillars were more obvious, which was more suitable for single cell research. The F-actin fluorescent intensity increased at the top of the micropillars. Moreover, the actin stress fibers of cells on the micropillar were aligned diagonally parallel to the gaps, while the cells on the flat had random orientation stress fibers (Fig. 6f), indicating that the cells rearranged cytoskeleton to fit the shape of the micropillar arrays. Compared to the well-defined filaments in cells grown on flat, H9c2 cells deformed on micropillar arrays displayed a quite diffuse actin network. We also carried out z-stack 3D scanning of the F-actin of H9c2 cells cultured on the micropillar arrays and flat plate, and restored cell growth morphology on the micropillar array by 3D reconstruction (see Method S2 of the 3D reconstruction method). The degree of red color indicates flatness, and the lighter the red color, the greater the thickness in the z-axis direction of cell growth. As shown in Fig. 6d, cells growing on ultramicromagnetic micropillars were more stereoscopic than those on PDMS micropillars. The mean fluorescence intensity of F-actin in cells grown on magnetic micropillar was relatively higher than those on pure PDMS micropillar, as shown in Fig. 6e. These data suggested that ultramicromagnetic fields could mitigate the degradation of the cytoskeleton protein (F-actin) caused by micropillars.

3.6. The expression of α-actinin, and Connexin-43 in cells on ultramicromagnetic micropillar arrays

We evaluated the differences in cardiac marker expressions to investigate the effects of ultramicromagnetic micropillar on the function of H9c2 cells by measuring connexin-43 (Cx43) and cardiac α-sarcomeric actinin (α-actinin). Cx43 is the most ubiquitously expressed gap junction protein to facilitate cell-cell communication. α-actinin is the cardiac-specific contractile protein involved in the actin-myosin contraction complex. As shown in Fig. 7a–c, α-actinin and Cx43 were downregulated in micropillar groups compared to that in the flat group. Ultramicromagnetic micropillar showed more α-actinin expression than pure PDMS-Pillar (Fig. 7d). The same results were obtained by capillary-based immunoassay (Fig. 7f). These data suggested that ultramicromagnetic micropillars ameliorate the contractility of H9c2 cells compared to pure PDMS micropillars. As opposed to the uniform distribution on the flat substrates, Cx43 on the micropillars accumulated at the top of the pillar. The communication between adjacent muscle cells is mainly carried out by Cx43. Our results indicated reduced cell–cell interactions in micropillar culture conditions manifested through the low expression of Cx43. Micropillars can separate cells and allow them to grow relatively independently, enabling the study of single cells.

3.7. The ROS production in cells on ultramicromagnetic micropillar array

ROS act as an important physiological signaling molecule in cell proliferation, differentiation, and motility [37]. It has been recognized as crucial regulators of actin dynamics [38]. Therefore, we have detected ROS levels in cells grown on flat and micropillar substrates by using a DCFH-DA fluorescent probe. The results showed that the cells grown on the micropillar had higher ROS levels than those on the flat substrates. However, the production of ROS in the ultramicromagnetic micropillar group was significantly reduced than that in the PDMS micropillar (Fig. 8a). ROS produced by cells growing on different substrates were quantitatively analyzed by Flow cytometer, and the results were consistent with those obtained by fluorescence microscopy (Fig. 8b and c). These data indicated that micropillars induced F-actin depolymerization is associated with ROS levels, and ultramicromagnetic micropillars can significantly reduce the production of ROS to facilitate cell growth and proliferation.

4. Discussion

Cells can sense and respond to substrate topography, which can

significantly affect cellular biological function [8,17,39]. In this study, we have investigated the biophysical and biochemical characteristics tuning of H9c2 cells grown on ultramicromagnetic micropillars. We found that ultramicromagnetic micropillars can modify the biochemical characteristics of cells induced by topography but not the biophysical characteristics (which due to the macroscopic scale parameters may not be sensitive enough to reflect the influence of ultramicromagnetic fields). The H9c2 cells grown on micropillars exhibited elongated morphology, reduced cell proliferation, deformed nuclei, increased adhesion and decreased cell cytoskeletal. However, cells grown on ultramicromagnetic micropillars revealed ameliorative cell proliferation and augmented cell cytoskeletal, compared to PDMS micropillar arrays substrate. These phenomena can be attributed to the effects of the ultramicromagnetic fields. Some data confirmed the WMF can alter cell systems and functions [29,40]. Alanna et al. suggested that WMF exposure can alter new tissue formation as a potential therapeutic tool [28]. The NdFeB/PDMS ultramicromagnetic micropillar we fabricated can greatly weaken the inhibition of the substrate morphology on cell proliferation, which makes surface-like implants more biocompatible and more suitable for long-term function in the human body. We observed that micropillars lead to cytoskeletal remodeling, which can be further improved by ultramicromagnetic micropillars. Additionally, we have presented the expression of α-actinin and Cx43, which played a critical role in cell contraction and cell-cell communication. The results showed that the ultramicromagnetic micropillar could improve decreased expression of α-actinin induced by the micropillar arrays. The α-actinin most acts as cross-linking F-actin and anchoring F-actin to the cytomembrane for cell-cell and cell-matrix junction [41]. Therefore, the effect of ultramicromagnetic field on cells is mainly reflected in facilitating communication between cells. Cells growing on the micropillar structure are in a relatively independent state, and the connections between cells are reduced, but this phenomenon can be improved by the increased expression of the cytoskeletal proteins modified with the ultramicromagnetic micropillar field. The problem of reduced intercellular communication caused by normal micropillars can be solved by dynamic ultramicromagnetic micropillars tuning (such as micropillar dimensions and NdFeB particle concentrations). The nucleation, polymerization, branching, and crosslinking of actin filament are highly regulated by extracellular and intracellular signal [42]. Actin itself is susceptible to oxidation by ROS and affects its function [43]. To understand the mechanism that how the ultramicromagnetic micropillar affected cytoskeletal remodeling, we observed their ROS levels respectively, as ROS overloading has been associated with F-actin degradation [44,45]. Based on the results of the flow cytometry analysis, it was observed that ultramicromagnetic micropillars had the ability to ameliorate the ROS level induced by micropillars and promoted the polymerization of F-actin. Actin oxidation causes decreased inter-actin contacts leading to F-actin disassembly [36]. The resulting actin monomers recombine more slowly, and fragment more easily once reassembled [46]. ROS have the capacity to induce modifications in protein function (extracellular signal-regulated kinase, nuclear factor kappa B, phosphatidylinositol-3 kinase/protein kinase B pathway et al. [47]), as well as structural alterations, thereby exerting influence over a plethora of signaling cascades. Upon stimulation of the relevant receptors and ligands, various downstream effector proteins are activated, consequently governing cellular growth, apoptosis, and proliferation [48]. The accumulation of excess ROS is detrimental for the cell growth and survival, as it leads to damage to cellular membranes, proteins, and DNA, ultimately impairing cell behavior [49]. Consistent with the results of previous studies, our study shows that ultramicromagnetic field ($\approx$ 80 μT) can change in cell behavior when applied to micropillar substrates, with its primary effect being reflected in the reduction of ROS levels and alterations in the expression of biological molecules.

The discernible influence exerted by magnetic micropillars upon cells primarily stems from the static magnetic field (SMF) they generate. The extent of alignment observed in cell structures when subjected to an
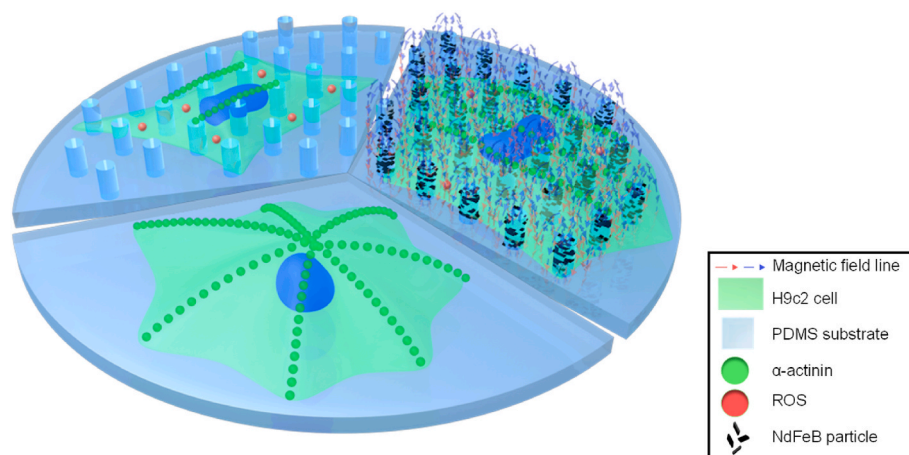
Fig. 9. Schematic illustrations of cell response to the coupling of static ultramicromagnetic field with micropillar substrate. Cells cultured on micropillars displayed distinct characteristics, including nucleus deformation, enhanced adhesion, reduced cytoskeletal structure (F-actin and α-actinin), and elevated levels of ROS. By harnessing the ultramicromagnetic static field, it has been found that ultramicromagnetic micropillars can mitigate these negative effects.

SMF may be associated with the intracellular composition. Diamagnetic anisotropy of intracellular components is the most common factor for the cell orientation. Structures characterized by regular arrangements, such as cell membranes and cytoskeletons, exhibit pronounced anisotropy in their shape, consequently generating diamagnetic anisotropy. Within this context, the cytoskeleton, protein distribution (as actin filaments) [50–52], experience torques, subsequently leading to alterations in cell morphology [53]. In our study, the magnetic micropillars were found to modulate F-actin disturbances induced by these micropillars through the static magnetic field. It is noteworthy that one of the recognized mechanisms underlying the action of static magnetic fields (SMF) in biological systems is the formation of free radical pairs [54,55]. Exposure to a magnetic field induces electrons to transition into singlet or triplet states, contingent upon the type, strength, and orientation of the magnetic field. This transition results in varying concentrations of ROS [55]. In accordance with existing literature, our results align with the observation that cells cultured on magnetic micropillars exhibit reduced ROS production in comparison to cells grown on PDMS micropillars.

The ultramicromagnetic micropillar also provides a great tool for understanding how cardiac cells interact with the 3D environment. The results of the three-dimensional reconstruction showed that the cells grown on the micropillars had the higher height rather than tiled on the flat substrate. A simple strategy has been proposed to enable hiPSCs to form a large number of organoids in situ on micropillar arrays without cumbersome manual procedures [56,57]. That means when the ultramicromagnetic micropillar arrays with the function of promoting cell proliferation and differentiation are applied to organoids, the potential efficiency of generating 3D organoids will be greatly improved. The rapid development of single-cell technology has accelerated the discovery of many biological disciplines [58]. Micropillars have the ability to induce distinct boundaries between cells, making them ideal for single-cell research. This approach can be further enhanced by combining it with single-cell sequencing techniques such as Microwell-seq [59].

The essence of the magnetic micropillar array is composed of small magnets arranged in order, which can be used for mechanical research of cells by applying non-invasive mechanical stimulation to cells with an external magnetic field. Upon application of an external magnetic field, cells cultivated on an array comprising both magnetic and non-magnetic micropillars experience forces generated by the deflected magnetic pillars. Concurrently, non-magnetic pillars respond by deflecting in response to cellular traction. This setup serves as a valuable platform for investigating cellular responses when situated on micropillars [60]. Due

to its response to external magnetic fields, magnetic micropillars can be applied to drug delivery, droplet manipulation, cellular probe, and various functional surfaces [61]. Magnetic micropillar arrays can be flexibly programmed and reprogrammed into various local states by simply reading a matrix of binary digits. This versatility extends to applications ranging from microscale letters and millimeter-scale QR codes to Chinese characters, promising advancements in various forms of digital mechanical metasurfaces [62,63]. While magnetic micropillars have made significant strides, certain challenges still impede their full integration into the biomedical field. Future research should continue to explore their applications in drug delivery, human-computer interaction, biosensors, and other pertinent domains.

The magnetic micropillars functioned as flexible magnets for capturing micro-scaled 3D morphology, which can be integrated with Faraday's law of induction [64], thereby enabling them to operate as sensors capable of detecting signals produced by cellular behavior. It is worth noting that the ultramicromagnetic micropillars are not limited to specific sizing and spacing requirements. The effect of magnetic field on a cell depends on the cell type and the strength of the magnetic field [52]. In terms of cell proliferation, it is apparent that the magnetic field exerts a more pronounced influence on HeLa cells in comparison to its impact on H9c2 cells. However, when considering cell morphology, the micropillar size utilized in this study seems to have a lesser effect on the morphology of HeLa cells when contrasted with its impact on H9c2 cells. It's important to emphasize that the effect of a magnetic field on a given cell is contingent upon both the cell type and the strength of the magnetic field. Moreover, the distinct sizes of magnetic micropillars, designed to align with the respective cell sizes, potentially generate varying magnetic fields, thereby eliciting divergent effects on the cells (Fig. S5). In fact, micropillar dimensions can be dynamically adjusted based on the shape and properties of the cells they interact with, demonstrating their immense potential for a wide range of applications.

5. Conclusion

In this study, ultramicromagnetic micropillar arrays were fabricated with PDMS and NdFeB particles by molding from silicon wafers. Our investigation revealed the profound influence of these micropillars on the behavior of H9c2 cells, particularly when combined with an ultramicromagnetic field. Cells cultured on micropillars measuring 5 μm in diameter, 10 μm in length, and spaced 15 μm apart displayed distinct characteristics, including nucleus deformation, enhanced adhesion, and reduced cytoskeletal structure. Furthermore, the presence of the micropillar array resulted in a decrease in cytoskeletal organization,

attributed to elevated levels of ROS (Fig. 9). However, by harnessing the ultramicromagnetic static field, magnetic micropillars were found to mitigate these effects. These findings underscore the potential of magnetic micropillars in providing a suitable 3D microenvironment and precise magnetic stimulation for cells. Consequently, they represent a promising tool for detecting and modulating cellular behaviors, with broad applications in tissue engineering and the development of flexible sensors for in vitro cellular studies.

Authors' contributions

Yue Quan conducted the experiments, collected the data and wrote the manuscript. Yinning Zhou supervised the whole project, including Funding acquisition and manuscript editing. Yuxin Wang, Yu Liu, Sen Ding, Qian Zhao contributed some methodologies. Xiuping Chen, Haifeng Li, Zikang Tang, Bingpu Zhou contributed to the manuscript revision.

Declaration of competing interest

The authors declare that they have no known competing financial interests or personal relationships that could have appeared to influence the work reported in this paper.

Data availability

Data will be made available on request.

Acknowledgments

Appendix A. Supplementary data

Supplementary data to this article can be found online at https://doi.org/10.1016/j.mtbio.2023.100831.

References

[1] B. Wang, J. Shi, J. Wei, X. Tu, Y. Chen, Fabrication of elastomer pillar arrays with elasticity gradient for cell migration, elongation and patterning, Biofabrication 11 (2019), 045003, https://doi.org/10.1088/1758-5090/ab21b3.

[2] P.Y. Wang, H. Thissen, P. Kingshott, Modulation of human multipotent and pluripotent stem cells using surface nanotopographies and surface-immobilised bioactive signals: a review, Acta Biomater. 45 (2016) 31–59, https://doi.org/10.1016/j.actbio.2016.08.054.

[3] J. Carthew, H.H. Abdelmaksoud, K.J. Cowley, M. Hodgson-Garms, R. Elnathan, J. P. Spatz, J. Brugger, H. Thissen, K.J. Simpson, N.H. Voelcker, J.E. Frith, V. J. Cadarso, Next generation cell culture tools featuring micro- and nanotopographies for biological screening, Adv. Funct. Mater. 32 (2022), 2100881, https://doi.org/10.1002/adfm.202100881.

[4] C.S. Chen, J. Tan, J. Tien, Mechanotransduction at cell-matrix and cell-cell contacts, Annu. Rev. Biomed. Eng. 6 (2004) 275–302, https://doi.org/10.1146/annurev.bioeng.6.040803.140040.

[5] G. Tullii, F. Giona, F. Lodola, S. Bonfadini, C. Bossio, S. Varo, A. Desii, L. Criante, C. Sala, M. Pasini, C. Verpelli, F. Galeotti, M.R. Antognazza, High-aspect-ratio semiconducting polymer pillars for 3D cell cultures, ACS Appl. Mater. Interfaces 11 (2019) 28125–28137, https://doi.org/10.1021/acsami.9b08822.

[6] N.E. Oyunbaatar, A. Shanmugasundaram, D.W. Lee, Contractile behaviors of cardiac muscle cells on mushroom-shaped micropillar arrays, Colloids Surf. B Biointerfaces 174 (2019) 103–109, https://doi.org/10.1016/j.colsurfb.2018.10.058.

[7] N. Tusamda Wakhloo, S. Anders, F. Badique, M. Eichhorn, I. Brigaud, T. Petithory, M. Vassaux, J.L. Milan, J.N. Freund, J. Ruhe, P.M. Davidson, L. Pieuchot, K. Anselme, Actomyosin, vimentin and LINC complex pull on osteosarcoma nuclei to deform on micropillar topography, Biomaterials 234 (2020), 119746, https://doi.org/10.1016/j.biomaterials.2019.119746.

[8] X. Xu, L. Ma, Y. Wu, L. Tang, Micropillar-based culture platform induces epithelial-mesenchymal transition in the alveolar epithelial cell line, J. Biomed. Mater. Res. 106 (2018) 3165–3174, https://doi.org/10.1002/jbm.a.36511.

[9] S. Fan, L. Qi, J. Li, S. Liu, R. Li, T. Zhan, X. Li, D. Wu, P. Lau, B. Qiu, G. Bi, W. Ding, Accelerating neurite growth and directing neuronal connections constrained by 3D porous microtubes, Nano Lett. 22 (2022) 8991–8999, https://doi.org/10.1021/acs.nanolett.2c03232.

[10] J. Kim, W.J. Choi, S.H. Moon, J. Jung, J.K. Park, S.H. Kim, J.O. Lee, Micropillar arrays as potential drug screens: inhibition of micropillar-mediated activation of the FAK-Src-paxillin signaling pathway by the CK2 inhibitor CX-4945, Acta Biomater. 27 (2015) 13–20, https://doi.org/10.1016/j.actbio.2015.08.041.

[11] Z. Jahed, R. Zareian, Y.Y. Chau, B.B. Seo, M. West, T.Y. Tsui, W. Wen, M.R. Mofrad, Differential collective- and single-cell behaviors on silicon micropillar arrays, ACS Appl. Mater. Interfaces 8 (2016) 23604–23613, https://doi.org/10.1021/acsami.6b08668.

[12] I. Tonazzini, S. Meucci, P. Faraci, F. Beltram, M. Cecchini, Neuronal differentiation on anisotropic substrates and the influence of nanotopographical noise on neurite contact guidance, Biomaterials 34 (2013) 6027–6036, https://doi.org/10.1016/j.biomaterials.2013.04.039.

[13] S. Fan, L. Qi, J. Li, D. Pan, Y. Zhang, R. Li, C. Zhang, D. Wu, P. Lau, Y. Hu, G. Bi, W. Ding, J. Chu, Guiding the patterned growth of neuronal Axons and dendrites using anisotropic micropillar scaffolds, Adv. Healthcare Mater. 10 (2021), e2100094, https://doi.org/10.1002/adhm.202100094.

[14] M. Ghibaudo, J.M. Di Meglio, P. Hersen, B. Ladoux, Mechanics of cell spreading within 3D-micropatterned environments, Lab Chip 11 (2011) 805–812, https://doi.org/10.1039/c0lc00221f.

[15] J. Li, F. Zhang, L. Yu, N. Fujimoto, M. Yoshioka, X. Li, J. Shi, H. Kotera, L. Liu, Y. Chen, Culture substrates made of elastomeric micro-tripod arrays for long-term expansion of human pluripotent stem cells, J. Mater. Chem. B 5 (2017) 236–244, https://doi.org/10.1039/c6tb02246d.

[16] X. Liu, R. Liu, Y. Gu, J. Ding, Nonmonotonic self-deformation of cell nuclei on topological surfaces with micropillar array, ACS Appl. Mater. Interfaces 9 (2017) 18521–18530, https://doi.org/10.1021/acsami.7b04027.

[17] F. Badique, D.R. Stamov, P.M. Davidson, M. Veuillet, G. Reiter, J.N. Freund, C. M. Franz, K. Anselme, Directing nuclear deformation on micropillared surfaces by substrate geometry and cytoskeleton organization, Biomaterials 34 (2013) 2991–3001, https://doi.org/10.1016/j.biomaterials.2013.01.018.

[18] F. Viela, D. Granados, A. Ayuso-Sacido, I. Rodriguez, Biomechanical cell regulation by high aspect ratio nanoimprinted pillars, Adv. Funct. Mater. 26 (2016) 5599–5609, https://doi.org/10.1002/adfm.201601817.

[19] E. Tanasa, C. Zaharia, A. Hudita, I.C. Radu, M. Costache, B. Galateanu, Impact of the magnetic field on 3T3-E1 preosteoblasts inside SMART silk fibroin-based scaffolds decorated with magnetic nanoparticles, Mater. Sci. Eng., C 110 (2020), 110714, https://doi.org/10.1016/j.msec.2020.110714.

[20] K. Zhang, W.B. Ge, S.T. Luo, Z. Zhou, Y.L. Liu, Static magnetic field promotes proliferation, migration, differentiation, and AKT activation of periodontal ligament stem cells, Cells Tissues Organs 212 (2023) 317–326, https://doi.org/10.1159/000524291.

[21] E.C. Kim, R. Leesungbok, S.W. Lee, H.W. Lee, S.H. Park, S.J. Mah, S.J. Ahn, Effects of moderate intensity static magnetic fields on human bone marrow-derived mesenchymal stem cells, Bioelectromagnetics 36 (2015) 267–276, https://doi.org/10.1002/bem.21903.

[22] C.Y. Chang, W.Z. Lew, S.W. Feng, C.L. Wu, H.H. Wang, S.C. Hsieh, H.M. Huang, Static magnetic field-enhanced osteogenic differentiation of human umbilical cord-derived mesenchymal stem cells via matrix vesicle secretion, Int. J. Radiat. Biol. 96 (2020) 1207–1217, https://doi.org/10.1080/09553002.2020.1787545.

[23] S.Y. Ho, I.C. Chen, Y.J. Chen, C.H. Lee, C.M. Fu, F.C. Liu, H.H. Liou, Static magnetic field induced neural stem/progenitor cell early differentiation and promotes maturation, Stem Cell. Int. 2019 (2019), 8790176, https://doi.org/10.1155/2019/8790176.

[24] A. Tampieri, E. Landi, F. Valentini, M. Sandri, T. D'Alessandro, V. Dediu, M. Marcacci, A conceptually new type of bio-hybrid scaffold for bone regeneration, Nanotechnology 22 (2011), 015104, https://doi.org/10.1088/0957-4484/22/1/015104.

[25] I.A. Paun, R.C. Popescu, B.S. Calin, C.C. Mustaciosu, M. Dinescu, C.R. Luculescu, 3D biomimetic magnetic structures for static magnetic field stimulation of osteogenesis, Int. J. Mol. Sci. 19 (2018), https://doi.org/10.3390/ijms19020495.

[26] D. Wu, X. Chang, J. Tian, L. Kang, Y. Wu, J. Liu, X. Wu, Y. Huang, B. Gao, H. Wang, G. Qiu, Z. Wu, Bone mesenchymal stem cells stimulation by magnetic nanoparticles and a static magnetic field: release of exosomal miR-1260a improves osteogenesis and angiogenesis, J. Nanobiotechnol. 19 (2021) 209, https://doi.org/10.1186/s12951-021-00958-6.

[27] M. Woods, F. Bobanovic, D. Brown, D.R. Alexander, Lyn and Syk tyrosine kinases are not activated in B-lineage lymphoid cells exposed to low-energy electromagnetic fields, Faseb. J. 14 (2000) 2284–2290, https://doi.org/10.1096/fj.00-0164com.

[28] A.V. Van Huizen, J.M. Morton, L.J. Kinsey, D.G. Von Kannon, M.A. Saad, T. R. Birkholz, J.M. Czajka, J. Cyrus, F.S. Barnes, W.S. Beane, Weak magnetic fields alter stem cell-mediated growth, Sci. Adv. 5 (2019), https://doi.org/10.1126/sciadv.aau7201. ARTN eaau7201.

[29] H. Gurhan, R. Bruzon, S. Kandala, B. Greenebaum, F. Barnes, Effects induced by a weak static magnetic field of different intensities on HT-1080 Fibrosarcoma cells, Bioelectromagnetics 42 (2021) 212–223, https://doi.org/10.1002/bem.22332.

[30] J. Kim, J. Park, K. Na, S. Yang, J. Baek, E. Yoon, S. Choi, S. Lee, K. Chun, J. Park, S. Park, Quantitative evaluation of cardiomyocyte contractility in a 3D

microenvironment, J. Biomech. 41 (2008) 2396–2401, https://doi.org/10.1016/j.jbiomech.2008.05.036.

[31] C.H. Seo, H. Jeong, Y. Feng, K. Montagne, T. Ushida, Y. Suzuki, K.S. Furukawa, Micropit surfaces designed for accelerating osteogenic differentiation of murine mesenchymal stem cells via enhancing focal adhesion and actin polymerization, Biomaterials 35 (2014) 2245–2252, https://doi.org/10.1016/j.biomaterials.2013.11.089.

[32] S. Ding, M.R. Wang, H. Yang, F.M. Hu, Z.Y. Dai, M. Lei, Q. Zhou, D.Z. Zhao, Y. B. Gao, J.W. Zhong, J.Y. Luo, B.P. Zhou, Sweeping-responsive interface using the intrinsic polarity of magnetized micropillars for self-powered and high-capacity human-machine interaction, Nano Energy 102 (2022), https://doi.org/10.1016/j.nanoen.2022.107671. ARTN 107671.

[33] V. Iacovacci, G. Lucarini, C. Innocenti, N. Comisso, P. Dario, L. Ricotti, A. Menciassi, Polydimethylsiloxane films doped with NdFeB powder: magnetic characterization and potential applications in biomedical engineering and microrobotics, Biomed. Microdevices 17 (2015), https://doi.org/10.1007/s10544-015-0024-0.

[34] R.L. Liu, O. Liu, Z. Pan, X.N. Liu, J.D. Ding, Cell type and nuclear size dependence of the nuclear deformation of cells on a micropillar array, Langmuir 35 (2019) 7469–7477, https://doi.org/10.1021/acs.langmuir.8b02510.

[35] X.N. Liu, R.L. Liu, Y.X. Gu, J.D. Ding, Nonmonotonic self-deformation of cell nuclei on topological surfaces with micropillar array, Acs Appl Mater Inter 9 (2017) 18521–18530, https://doi.org/10.1021/acsami.7b04027.

[36] Q. Xu, L.P. Huff, M. Fujii, K.K. Griendling, Redox regulation of the actin cytoskeleton and its role in the vascular system, Free Radic. Biol. Med. 109 (2017) 84–107, https://doi.org/10.1016/j.freeradbiomed.2017.03.004.

[37] T. Finkel, Signal transduction by reactive oxygen species, J. Cell Biol. 194 (2011) 7–15, https://doi.org/10.1083/jcb.201102095.

[38] M.C.W. Oswald, N. Garnham, S.T. Sweeney, M. Landgraf, Regulation of neuronal development and function by ROS, FEBS Lett. 592 (2018) 679–691, https://doi.org/10.1002/1873-3468.12972.

[39] G. Lee, Y. Cho, E.H. Kim, J.M. Choi, S.S. Chae, M.G. Lee, J. Kim, W.J. Choi, J. Kwon, E.H. Han, S.H. Kim, S. Park, Y.H. Chung, S.G. Chi, B.H. Jung, J.H. Shin, J. O. Lee, Pillar-based mechanical induction of an Aggressive tumorigenic lung cancer cell model, ACS Appl. Mater. Interfaces 14 (2022) 20–31, https://doi.org/10.1021/acsami.1c12380.

[40] S.V. Surma, G.B. Belostotskaya, B.F. Shchegolev, V.E. Stefanov, Effect of weak static magnetic fields on the development of cultured skeletal muscle cells, Bioelectromagnetics 35 (2014) 537–546, https://doi.org/10.1002/bem.21876.

[41] L. Matt, K. Kim, A.C. Hergarden, T. Patriarchi, Z.A. Malik, D.K. Park, D. Chowdhury, O.R. Buonarati, P.B. Henderson, C. Gokcek Sarac, Y. Zhang, D. Mohapatra, M.C. Horne, J.B. Ames, J.W. Hell, Alpha-actinin Anchors PSD-95 at postsynaptic sites, Neuron 97 (2018) 1094–1109, https://doi.org/10.1016/j.neuron.2018.01.036, e1099.

[42] D.A. Fletcher, R.D. Mullins, Cell mechanics and the cytoskeleton, Nature 463 (2010) 485–492, https://doi.org/10.1038/nature08908.

[43] C. Wilson, J.R. Terman, C. Gonzalez-Billault, G. Ahmed, Actin filaments-A target for redox regulation, Cytoskeleton (Hoboken) 73 (2016) 577–595, https://doi.org/10.1002/cm.21315.

[44] H. Zhou, J. Wang, S.Y. Hu, H. Zhu, S. Toanc, J. Ren, BI1 alleviates cardiac microvascular ischemia-reperfusion injury via modifying mitochondrial fission and inhibiting XO/ROS/F-actin pathways, J. Cell. Physiol. 234 (2019) 5056–5069, https://doi.org/10.1002/jcp.27308.

[45] D. Stojkov, P. Amini, K. Oberson, C. Sokollik, A. Duppenthaler, H.U. Simon, S. Yousefi, ROS and glutathionylation balance cytoskeletal dynamics in neutrophil extracellular trap formation, JCB (J. Cell. Biol.) 216 (2017) 4073–4090, https://doi.org/10.1083/jcb.201611168.

[46] E.E. Grintsevich, H.G. Yesilyurt, S.K. Rich, R.J. Hung, J.R. Terman, E. Reisler, F-actin dismantling through a redox-driven synergy between Mical and cofilin, Nat. Cell Biol. 18 (2016) 876–885, https://doi.org/10.1038/ncb3390.

[47] X.T. Zhang, J. Hu, L.H. Su, C.A. Geng, J.J. Chen, Artematrolide A inhibited cervical cancer cell proliferation via ROS/ERK/mTOR pathway and metabolic shift, Phytomedicine 91 (2021), https://doi.org/10.1016/j.phymed.2021.153707. ARTN 153707.

[48] L. Diebold, N.S. Chandel, Mitochondrial ROS regulation of proliferating cells, Free Radic. Biol. Med. 100 (2016) 86–93, https://doi.org/10.1016/j.freeradbiomed.2016.04.198.

[49] L. Kma, T.J. Baruah, The interplay of ROS and the PI3K/Akt pathway in autophagy regulation, Biotechnol. Appl. Biochem. 69 (2022) 248–264, https://doi.org/10.1002/bab.2104.

[50] Z. Wang, F. Hao, C. Ding, Z. Yang, P. Shang, Effects of static magnetic field on cell biomechanical property and membrane ultrastructure, Bioelectromagnetics 35 (2014) 251–261, https://doi.org/10.1002/bem.21847.

[51] L. Dini, L. Abbro, Bioeffects of moderate-intensity static magnetic fields on cell cultures, Micron 36 (2005) 195–217, https://doi.org/10.1016/j.micron.2004.12.009.

[52] B. Zhang, X.C. Yuan, H.H. Lv, J.M. Che, S.H. Wang, P. Shang, Biophysical mechanisms underlying the effects of static magnetic fields on biological systems, Prog. Biophys. Mol. Biol. 177 (2023) 14–23, https://doi.org/10.1016/j.pbiomolbio.2022.09.002.

[53] W. Bras, J. Torbet, G.P. Diakun, G.L. Rikken, J.F. Diaz, The diamagnetic susceptibility of the tubulin dimer, J Biophys 2014 (2014), 985082, https://doi.org/10.1155/2014/985082.

[54] C.B. Grissom, Magnetic-field effects in biology - a survey of possible mechanisms with emphasis on radical-pair recombination, Chem. Rev. 95 (1995) 3–24, https://doi.org/10.1021/cr00033a001.

[55] A.V. Van Huizen, J.M. Morton, L.J. Kinsey, D.G. Von Kannon, M.A. Saad, T. R. Birkholz, J.M. Czajka, J. Cyrus, F.S. Barnes, W.S. Beane, Weak magnetic fields alter stem cell-mediated growth, Sci. Adv. 5 (2019), https://doi.org/10.1126/sciadv.aau7201 eaau7201.

[56] Y.J. Zhu, L. Wang, H. Yu, F.C. Yin, Y.Q. Wang, H.T. Liu, L. Jiang, J.H. Qin, In situ generation of human brain organoids on a micropillar array, Lab Chip 17 (2017) 2941–2950, https://doi.org/10.1039/c7lc00682a.

[57] Y.Q. Wang, H. Wang, P.W. Deng, W.W. Chen, Y.Q. Guo, T.T. Tao, J.H. Qin, In situ differentiation and generation of functional liver organoids from human iPSCs in a 3D perfusable chip system, Lab Chip 18 (2018) 3606–3616, https://doi.org/10.1039/c8lc00869h.

[58] K.D. Zimmerman, M.A. Espeland, C.D. Langefeld, A practical solution to pseudoreplication bias in single-cell studies, Nat. Commun. 12 (2021), https://doi.org/10.1038/s41467-021-21038-1. ARTN 738.

[59] J. He, Y.X. Lin, M. Meng, J.Q. Li, J.Y.H. Yang, H. Wang, Construction of a human cell landscape of COVID-19 infection at single-cell level, Aging Dis 12 (2021) 705–709, https://doi.org/10.14336/Ad.2021.0301.

[60] N.J. Sniadecki, A. Anguelouch, M.T. Yang, C.M. Lamb, Z. Liu, S.B. Kirschner, Y. Liu, D.H. Reich, C.S. Chen, Magnetic microposts as an approach to apply forces to living cells, P Natl Acad Sci USA 104 (2007) 14553–14558, https://doi.org/10.1073/pnas.0611613104.

[61] K. Ni, Z.Z. Wang, Recent progress on the development of magnetically-responsive micropillars: Actuation, fabrication, and applications, Adv. Funct. Mater. 33 (2023), https://doi.org/10.1002/adfm.202213350.

[62] Z. Wang, Digital mechanical metasurfaces for reprogrammable structural display, ACS Nano 17 (2023) 10078–10089, https://doi.org/10.1021/acsnano.2c12679.

[63] K. Ni, Q. Peng, E.L. Gao, K. Wang, Q. Shao, H.B. Huang, L.J. Xue, Z.Z. Wang, Core-shell magnetic micropillars for reprogrammable Actuation, ACS Nano 15 (2021) 4747–4758, https://doi.org/10.1021/acsnano.0c09298.

[64] Q. Zhou, B. Ji, F.M. Hu, Z.Y. Dai, S. Ding, H. Yang, J.W. Zhong, Y.C. Qiao, J. H. Zhou, J.Y. Luo, B.P. Zhou, Magnetized microcilia array-based self-powered electronic skin for micro-scaled 3D morphology recognition and high-capacity communication, Adv. Funct. Mater. 32 (2022), https://doi.org/10.1002/adfm.202208120. ARTN 2208120.